

Banner appropriate to article type will appear here in typeset article

# The relationship between manipulated inter-scale phase and energy-efficient turbulent drag reduction

Rahul Deshpande<sup>1</sup>†, Dileep Chandran<sup>1</sup>, Alexander J. Smits<sup>2</sup>, and Ivan Marusic<sup>1</sup>

<sup>1</sup>Dept. Mechanical Engg., University of Melbourne, Parkville, VIC 3010, Australia

<sup>2</sup>Dept. Mechanical and Aerospace Engg., Princeton University, Princeton, NJ 08544, USA

(Received xx; revised xx; accepted xx)

We investigate the mechanism responsible for the high-Reynolds number skin-friction drag reduction strategy reported by Marusic *et al.* (2021). The strategy involves imposing relatively low-frequency streamwise travelling waves of spanwise velocity at the wall to actuate the drag generating outer-scales. This approach has proven to be more energy-efficient than the conventional method of directly targeting the drag producing inner-scales, which typically requires actuation at higher frequencies. We find that both pathways yield drag reduction with an accompanying broadband attenuation of the wall-shear stress spectrum and modified inter-scale phase relationships. Statistics such as the amplitude modulation coefficient and skewness of the streamwise velocity, which represent the average measures of phase between the triadically consistent scales, reveal that higher drag reduction is associated with enhanced coupling between the inner and outer scales. This enhancement is reflected in a reduction of their inter-scale phase difference. Hence, actuating the outer-scales at low frequencies leads to a substantial attenuation of the major drag producing inner-scales. This energy-efficient strategy to achieve drag reduction is expected to further improve at very high Reynolds numbers, where inner-outer couplings have been found to strengthen naturally.

**Key words:** turbulent boundary layers, boundary layer control, drag reduction.

## 1. Introduction

A characteristic feature of any turbulent flow is the broad range of scales, or ‘eddies’, which carry the total kinetic energy. The eddies are coupled with each other non-linearly, and this non-linear ‘cross-talk’ across the energy spectrum is the cornerstone for the energy transfer process in a turbulent flow. Since the non-linearity in the governing Navier-Stokes equations is quadratic, this inter-scale coupling is, by definition, triadic in nature (Duvvuri & McKeon 2015). Here, triadically coupled

† Email address for correspondence: [raadeshpande@gmail.com](mailto:raadeshpande@gmail.com)

eddies correspond to the scenario when the time scales ( $T_i$ ) of any three eddies (say  $l$ ,  $m$  and  $n$ ) are related via either of the four relationships:

$$(i) \omega_l = \omega_m - \omega_n, (ii) \omega_l = \omega_m + \omega_n, (iii) \omega_l = 2\omega_m, (iv) \omega_l = 2\omega_n, \quad (1.1)$$

where the frequencies  $\omega_i = 2\pi/T_i$ .

In the case of wall-bounded turbulent flows, the nature of inter-scale coupling has been verified previously through a set of experiments and analysis by McKeon and co-workers (Jacobi & McKeon 2013, 2017; Duvvuri & McKeon 2015, 2017). The experiments involved artificial excitation of a large *outer-scaled* eddy, which spanned the boundary layer (consider for instance, eddy  $l$  in figure 1), by imposition of an oscillatory forcing via a dynamic roughness element. Statistical analysis of the velocity signals acquired within this perturbed boundary layer confirmed the influence of this forcing (with time scale,  $T_l$ ) on the corresponding small *inner-scaled* eddies  $m$  and  $n$  (figure 1(a)), which are triadically coupled with  $l$ . This coupling, or ‘cross-talk’, was found to be facilitated by a phase locking of the synthetic scale ( $\psi_l$ ) and the average triadic ‘envelope’ of the small scales ( $\psi_{\epsilon(m,n)}$ ), where  $\psi_i$  and  $\epsilon$  respectively denote the phase and the envelope.

As discussed by Duvvuri & McKeon (2015) and Jacobi & McKeon (2017), this inter-scale coupling offers an opportunity to control and manipulate the near-wall inner-scaled turbulence by exciting the triadically coupled outer-scales, with potential implications for drag reduction. For instance, the inner-scaled eddies near the wall are a major contributor to the total skin-friction drag across the practically-relevant Reynolds number range (Deck *et al.* 2014; Chandran *et al.* 2022). It is challenging, however, to actuate these eddies owing to their very small time/length scales in physical units (Ricco *et al.* 2021). Alternatively, it may be possible to leverage the coupling between the turbulent scales to indirectly attenuate these drag contributing inner-scales through their triadically coupled outer-scales.

In the present study, we test this idea by considering the flow-control approach of imposing spanwise wall-oscillations (Akhavan *et al.* 1993; Quadrio *et al.* 2009; Agostini *et al.* 2014; Ricco *et al.* 2021), wherein the oscillating wall elements are synchronized to generate an upstream traveling wave with respect to the mean flow direction. Figure 1(b) schematically describes this control strategy, where the instantaneous spanwise velocity ( $w_{wall}$ ) imposed on the wall is given by:  $w_{wall}(x, t) = A\sin(\kappa_x x - \omega_{osc}t)$ . Here,  $T_{osc} = 2\pi/\omega_{osc}$  and  $A$  are the time period and amplitude of the spanwise oscillation, respectively;  $\kappa_x = 2\pi/\lambda$  is the streamwise wavenumber of the traveling wave where  $\lambda$  is the wavelength;  $t$  denotes time; and  $u$ ,  $v$  and  $w$  denote the velocity fluctuations along the streamwise ( $x$ ), wall-normal ( $y$ ) and spanwise ( $z$ ) directions, respectively. This approach of imposing spanwise oscillations on the wall has been investigated extensively (refer to Ricco *et al.* (2021) and references therein), predominantly for its ability to achieve significant drag reduction (DR) through actuating the near-wall inner-scaled motions, which we refer to here as the *inner-scaled actuation* (ISA) strategy. These investigations have mostly been limited to low Reynolds number flows, for which the inner-scales are the dominant (if not sole) contributors to the total drag. Oscillating these wall elements at the associated small time scales, however, incurs a large power cost ( $\propto (T_{osc})^{-\frac{5}{2}}$ ; Quadrio & Ricco (2011)), making net power savings from the ISA strategy unlikely. Marusic *et al.* (2021), however, used the premise that outer-scale contributions to the turbulent skin-friction increase with Reynolds numbers to demonstrate that low-frequency spanwise wall-actuation targeting these outer-scales can also yield DR for a sufficiently high Reynolds number flow. More importantly, this *outer-scaled actuation* (OSA) strategy

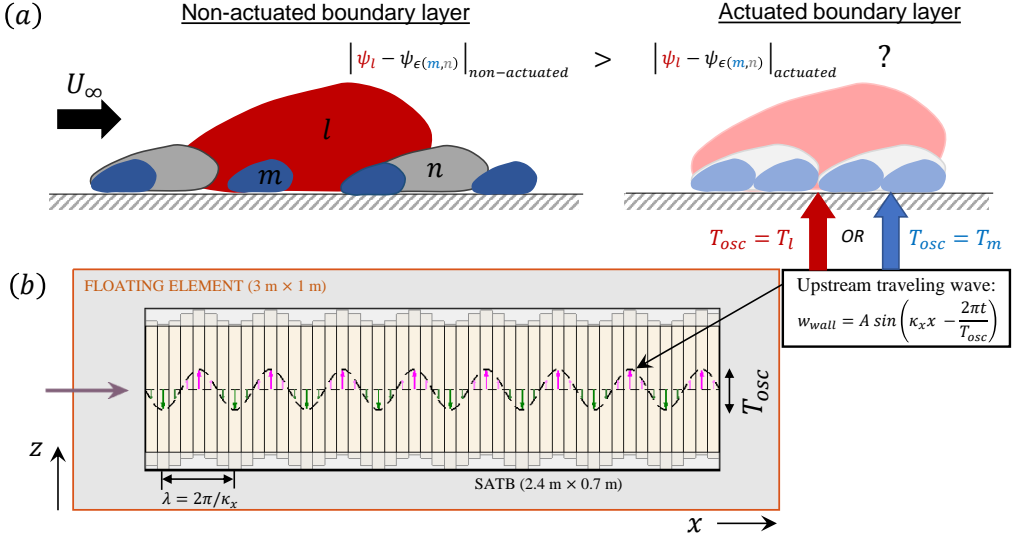


Figure 1: (a) Schematic representation of triadically coupled eddies ( $l$ ,  $m$ ,  $n$ ) with time scales  $T_l$ ,  $T_m$ ,  $T_n$  and phase  $\psi_l$ ,  $\psi_m$ ,  $\psi_n$ , respectively. (b) Schematic of the spanwise wall-actuation scheme investigated by Marusic *et al.* (2021) and others. The terminology is discussed in §1.

(Chandran *et al.* 2022) required considerably lower input power, thereby yielding drag reduction with net power savings.

The present study investigates whether this energy-efficient drag reduction via the OSA strategy is facilitated by the manipulation of the inter-scale phase of the triadically coupled inner- and outer-scales. To this end, statistical analysis, based on the arguments of McKeon and co-workers (Duvvuri & McKeon 2015; Jacobi & McKeon 2017), is conducted on the experimental data of Chandran *et al.* (2022). The same analysis is also extended for the ISA strategy to confirm whether the triadically coupled scales can be influenced from either end of the spectrum.

## 2. Experimental data

All experiments reported in this study were performed in the large wind tunnel (HRNBLWT) at the University of Melbourne. It features a  $3\text{m} \times 1\text{m}$  (length  $\times$  width) floating element balance (figure 1(b)) located approximately 20 m downstream from the start of the test section. The spanwise wall actuation test bed (SATB) is flush mounted in a rectangular cutout of  $2.7\text{ m} \times 0.7\text{ m}$  (length  $\times$  width) centred within this floating element. The SATB is a combination of 4 independently-controlled, servo motor driven machines that run in a phase-synchronised manner to impose a  $8\lambda$  long upstream travelling sinusoidal wave at the wall (figure 1(b)). This is made possible by discretising each machine into 12 slats (oscillating elements) which cumulatively span a length of  $2\lambda = 0.6\text{ m}$ , with their phase controlled by a central camshaft. These slats, along with the camshaft, were fabricated with a high degree of precision and tolerance, enabling a spanwise wall motion while maintaining a negligible gap ( $\sim 100\text{ }\mu\text{m}$ ) between the individual slats. The surfaces of the slats were polished to ensure a hydraulically smooth boundary layer flow for the non-actuated cases (Marusic *et al.* 2021). When actuated, the slats have a fixed half stroke length of  $d = 18\text{ mm}$  and can be oscillated at frequencies as high as  $1/T_{osc} = 25\text{ Hz}$ , leading to a maximum achievable spanwise velocity of  $A (= 2\pi d/T_{osc}) = 2.83\text{ m/s}$ . Further

TBL			Parameters associated with spanwise oscillations imposed on the wall						Drag reduction
$Re_{\tau_o}$	$U_{\infty}$ (m/s)	$\delta$ (m)	$1/T_{osc}$ (Hz)	$A$ (m/s)	$\kappa_x$ (1/m)	$T_{osc}^+ = \frac{T_{osc} U_{\tau_o}^2}{\nu}$	$A^+ = \frac{A}{U_{\tau_o}}$	$\kappa_x^+ = \frac{\kappa_x \nu}{U_{\tau_o}}$	DR(%)
<b>Non-actuated flow:</b>									
6 000	7	0.39	—	—	—	—	—	—	—
9 700	11	0.39	—	—	—	—	—	—	—
<b>Inner-scaled actuation (ISA; <math>T^+ \lesssim 350</math>):</b>									
6 000	7	0.39	10	1.13	20.94	348	4.9	0.0014	10%
6 000	7	0.39	15	1.70	20.94	232	7.4	0.0014	16%
6 000	7	0.39	20	2.26	20.94	174	9.8	0.0014	20%
6 000	7	0.39	25	2.83	20.94	140	12.3	0.0014	24%
<b>Outer-scaled actuation (OSA; <math>T^+ &gt; 350</math>):</b>									
9 700	11	0.39	10	1.13	20.94	906	3.0	0.0008	9.5%
9 700	11	0.39	15	1.70	20.94	604	4.6	0.0008	11.5%
9 700	11	0.39	20	2.26	20.94	453	6.2	0.0008	12.5%
9 700	11	0.39	25	2.83	20.94	362	7.8	0.0008	15%

Table 1: A summary of the experimental dataset employed in this study, originally reported in Marusic *et al.* (2021) and Chandran *et al.* (2022).

details regarding the characterization and validation of the SATB can be found in Marusic *et al.* (2021) and Chandran *et al.* (2022).

All velocity data analyzed in this study were acquired using hot-wire anemometry (table 1) for various non-actuated and actuated ( $140 \lesssim T_{osc}^+ \lesssim 906$ ) cases. The data were acquired over the SATB with an actuation length of at least  $2\lambda$ , beyond which the local drag, modified due to the actuation was found to have saturated (Chandran *et al.* 2022). The mean wall shear stress ( $\bar{\tau}_w$ ) for the non-actuated and actuated flow cases was measured directly using the floating element drag balance, and also estimated from dedicated hot-wire experiments conducted in the viscous sublayer. Additional description of these measurements can be found in Marusic *et al.* (2021) and Chandran *et al.* (2022), where the data are analysed in greater depth. The present analysis is limited to boundary layers at  $Re_{\tau_o} (= \delta U_{\tau_o} / \nu) \approx 6000$  and  $9700$ . Here,  $\delta$  is the boundary layer thickness,  $\rho$  and  $\nu$  are the density and kinematic viscosity, respectively, and  $U_{\tau_o} = \sqrt{\bar{\tau}_{w_o} / \rho}$  is the friction velocity of the non-actuated flow. The superscript ‘+’ will denote normalization in viscous units using  $\nu$  and  $U_{\tau_o}$ .

We investigate the inter-scale phase relationships for various ISA and OSA cases at these two Reynolds numbers by analyzing streamwise velocity fluctuations ( $u$ ), acquired by a normal hot-wire positioned at  $4.5 \lesssim y^+ \lesssim 6$  (where  $y^+ = y U_{\tau_o} / \nu$ ). This  $y^+$ -range was deemed optimal in a way that is close enough to the wall, for the  $u$ -signal to be sensitive to spanwise wall oscillations, while also being far enough to have a substantial streamwise variance,  $\bar{u}^2$ , for a greater signal-to-noise ratio (overbar denotes time averaging). Following Marusic *et al.* (2021), we consider all experiments with  $T_{osc}^+ \lesssim 350$  to be associated with ISA strategy, while those with  $T_{osc}^+ \gtrsim 350$  are associated with the OSA strategy, and  $T_c^+ = 350$  is taken to be the nominal demarcation between inner and outer scales.

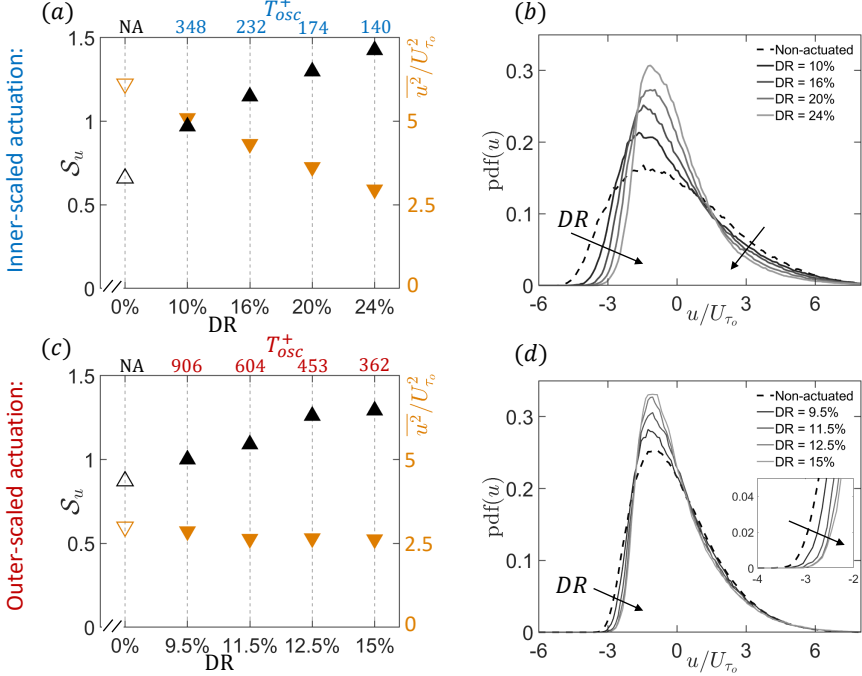


Figure 2: (a,c) Variance ( $\overline{u^2}$ ), skewness ( $\mathcal{S}_u$ ) and (b,d) probability distribution function of the  $u$ -fluctuations corresponding to various (a,b) ISA ( $y^+ \sim 6$ ) and (c,d) OSA cases ( $y^+ \sim 4.5$ ). In (a,c), DR = 0% or  $T_{osc}^+ = \text{NA}$  refers to the non-actuated case (denoted by empty symbols).  $\overline{u^2}$  in (a,c) and  $u$ -fluctuations in (b,d) are normalized by  $U_{\tau_0}$ . Note that the abscissa is not linear.

### 3. Results

#### 3.1. Mean phase between all triadically coupled scales

Duvvuri & McKeon (2015) showed that the phase relationships between triadically coupled scales (coexisting at  $y$ ) can be estimated by computing the skewness of the streamwise velocity fluctuations ( $\mathcal{S}_u$ ) at  $y$ . This was demonstrated by decomposing the experimentally acquired, statistically stationary  $u$ -time series ( $u(t)$ ) as a summation of its Fourier modes, i.e.  $u(t) = \sum_{i=1}^{\infty} \alpha_i \sin(\omega_i t + \psi_i)$ , with circular frequencies  $\omega_i$  ( $= 2\pi/T_i$ ), amplitudes ( $\alpha_i$ ), phase ( $\psi_i$ ) and  $0 < \omega_i < \omega_{\infty}$ . That is,

$$\mathcal{S}_u = \frac{\overline{u^3}}{\sigma^3} = \frac{6}{4\sigma^3} \sum_{\substack{\forall l,m,n \\ \omega_l < \omega_m < \omega_n \\ \omega_l + \omega_m = \omega_n}} \alpha_l \alpha_m \alpha_n \sin(\psi_l + \psi_m - \psi_n) + \frac{3}{4\sigma^3} \sum_{\substack{l=1 \\ \omega_n = 2\omega_l}} \alpha_l^2 \alpha_n \sin(2\psi_l - \psi_n), \quad (3.1)$$

where  $\sigma = \sqrt{\overline{u^2}}$ , and  $\psi_l + \psi_m - \psi_n$  represents the phase difference between the triadically consistent scales, existing across the energy spectrum:  $0 < \omega_i < \omega_{\infty}$ . Hence,  $\mathcal{S}_u$  can be considered as a surrogate of the average measure for the phase between the various turbulent eddies/scales coexisting at  $y$ .

Figures 2(a,c) display our results for the near-wall values of  $\overline{u^2}$  and  $\mathcal{S}_u$ . As expected, in scenarios of drag reduction, near-wall  $\overline{u^2}$  reduces with increases in DR for both ISA and OSA cases (Chandran *et al.* 2022). The degree of reduction, however, is more gradual for OSA cases than for ISA cases, and it appears to be directly related to the amount of drag reduction. We note that the OSA cases considered here have

relatively lower  $A^+$  levels when compared to the ISA cases (table 1). This trend confirms that  $u$  near the wall is indeed influenced by wall actuation and hence, can be used to understand the change in flow physics with DR.

We also see that  $\mathcal{S}_u$  increases with DR for both ISA and OSA cases, indicating that an increase in DR is associated with an average decrease in phase between the triadically consistent scales (see also Duvvuri & McKeon (2015)). The probability distribution functions (*pdf*) for the various  $u$ -signals, shown in figures 2(b,d), indicate that this trend is coupled with the reduction in intense  $-u$  events ( $u/U_{\tau_o} \lesssim -3$ ). For the ISA cases this can be associated with weakening of the low-speed near-wall streaks, as noted in some earlier works (Akhavan *et al.* 1993; Agostini *et al.* 2014; Ricco *et al.* 2021), but that a similar result can be observed for the OSA cases has only been noted recently by Chandran *et al.* (2022), based on near-wall PIV measurements.

### 3.2. Mean phase between triadically coupled inner and outer scales

Whether this reduction in intense  $-u$  events, for the cases of OSA, exists due to the attenuation of viscosity-dominated near-wall (inner) scales, or that of the inertia-dominated outer eddies, can be understood by computing the individual inner ( $u_i$ ) and outer ( $u_o$ ) contributions to the  $u$ -fluctuations. In particular, we can investigate the change in mean phase between the outer ( $u_o = u(T^+ \gtrsim T_c^+)$ ) and the inner scales ( $u_i = u(T^+ \lesssim T_c^+)$ ), where  $T_c^+ = \frac{2\pi}{\omega_c^+} = 350$ . For this, we follow Mathis *et al.* (2011) and linearly decompose  $u = u_o + u_i$  to obtain

$$\mathcal{S}_u = \frac{\overline{u^3}}{\sigma^3} = \overline{\overline{u_o^3}} + \overline{\overline{u_i^3}} + 3\overline{\overline{u_o^2 u_i}} + 3\overline{\overline{u_i^2 u_o}}, \quad (3.2)$$

where the double overbar denotes a time averaged quantity normalized by  $\sigma^3$ . Duvvuri & McKeon (2015) reported exact expressions for the four individual terms given in (3.2), where

$$\overline{\overline{u_i^2 u_o}} = \frac{1}{2\sigma^3} \sum_{\substack{\forall l, m, n \\ \omega_n - \omega_m = \omega_l \\ 0 < \omega_l < \omega_c \\ \omega_m, \omega_n > \omega_c}} \alpha_l \alpha_m \alpha_n \sin(\psi_l + \psi_m - \psi_n), \quad (3.3)$$

meaning that the cross-term  $3\overline{\overline{u_i^2 u_o}}$  represents the mean phase difference between the outer-scale  $\omega_l$  and the ‘envelope’ of the triadically coupled inner-scales  $\omega_n, \omega_m$ . Enhanced values for this cross-term can therefore be correlated with a reduction in phase between the outer and inner scales. Theoretically, the term  $3\overline{\overline{u_o^2 u_i}}$  also represents an inner-outer coupling in some form, but Mathis *et al.* (2011) found that its contributions to  $\mathcal{S}_u$  were negligible for a canonical boundary layer.

The four decomposed terms of  $\mathcal{S}_u$  (3.2) for the various cases are shown in figures 3(a) and 3(d). We conclude that the increase in  $\mathcal{S}_u$  with DR can be attributed predominantly to two terms: (i)  $\overline{\overline{u_i^3}}$ , which represents the average phase between the triadically coupled inner scales ( $T^+ < 350$ ), and (ii)  $3\overline{\overline{u_i^2 u_o}}$ , the cross-term that represents the average phase between the outer scales and the envelope of the triadically coupled inner-scales (3.3). An increase in  $3\overline{\overline{u_i^2 u_o}}$  with DR suggests that drag reduction is associated with a decrease in the average phase difference between  $u_o$  and  $u_i$  (Duvvuri & McKeon 2015). In the case of ISA, the *pdf* plots for the  $u_i$  and  $u_o$  signals (figures 3(b,c)) show a reduction in intense  $-u_i$  events with an increase in

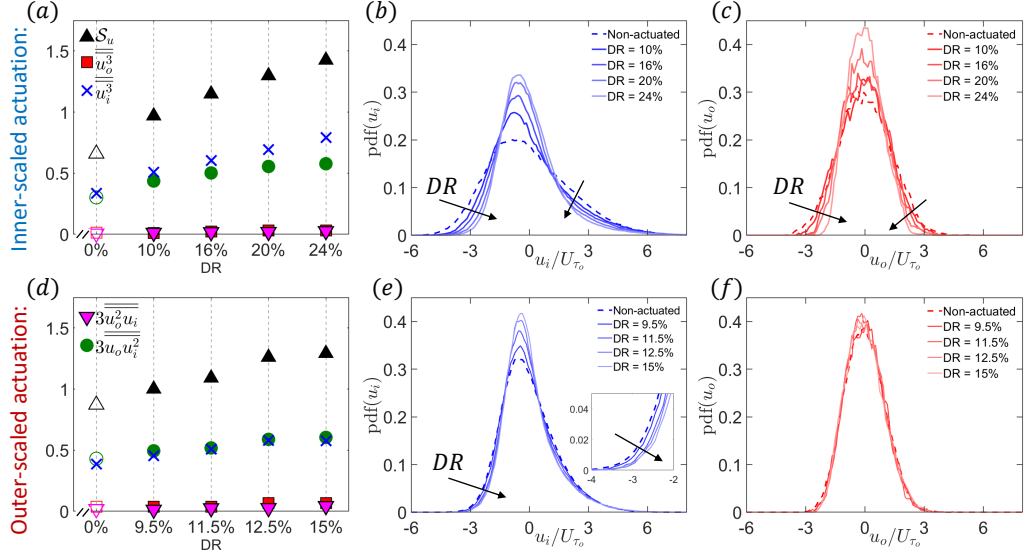


Figure 3: (a,d) Terms obtained from decomposition of skewness ( $S_u$ ) corresponding to various (a) ISA and (d) OSA cases documented in table 1, noting that the abscissa is not linear. Probability distribution functions of the (b,e) inner-scale and (c,f) outer-scale sub-components of  $u$ , corresponding to the same (b,c) ISA and (e,f) OSA cases as in (a,d). In (a,d), DR = 0% refers to the non-actuated case.

DR, which suggests the weakening of near-wall low-speed streaks. But this process is also accompanied by a reduction in intense  $-u_o$  and  $+u_o$  events, indicating an enhanced inter-scale communication between the inner and outer scales. Similarly, in the case of OSA (figures 3(e,f)), the intense  $-u_i$  events are attenuated much more significantly than the corresponding  $u_o$  events. The substantial drag reduction noted in the cases of both ISA and OSA strategies, thus, is a consequence of the attenuation of both – the inner and outer scales – which contribute to the total drag. This is investigated further in the next section by examining the changes to the scale-specific energy (i.e. the  $u$ -spectra) due to spanwise wall-actuation.

### 3.3. Scale-specific phase between inner and outer scales

Figures 4(c,d) show the premultiplied  $u$ -spectra,  $f\phi_{uu}^+$  for the non-actuated and actuated cases, where figure 4(c) represents the ISA strategy ( $T_{osc}^+ = 232$ ) and figure 4(d) represents the OSA strategy ( $T_{osc}^+ = 604$ ). Here,  $\phi_{uu}^+ = \langle \tilde{u}(T^+) (\tilde{u}^*(T^+)) \rangle / U_{\tau_o}^2$ , and ‘ $\sim$ ’ represents the Fourier transform in time while ‘ $\langle \rangle$ ’ indicates ensemble averaging and ‘ $*$ ’ indicates the complex conjugate. The spectra for both actuated cases are attenuated across the inner ( $T^+ \lesssim 350$ ) as well as outer ( $T^+ \gtrsim 350$ ) scales, and not localized to a specific scale range depending on the actuation time scale (ISA or OSA). Such broadband attenuation of the near-wall  $u$ -spectra, in case of the ISA strategy, is also observed in previously published simulation data at low Reynolds numbers (Gatti *et al.* 2018), but the results at high Reynolds numbers are new. This broadband attenuation affects a large range of energetic scales (indicated by the grey background), which are known to co-exist between the inner and outer peaks of the  $u$ -spectrogram of a non-actuated boundary layer (shown in figures 4(a,b) with cross and circle symbols, respectively). The substantial drag reduction, which is made possible via the energy attenuation across a broad scale range, can therefore be

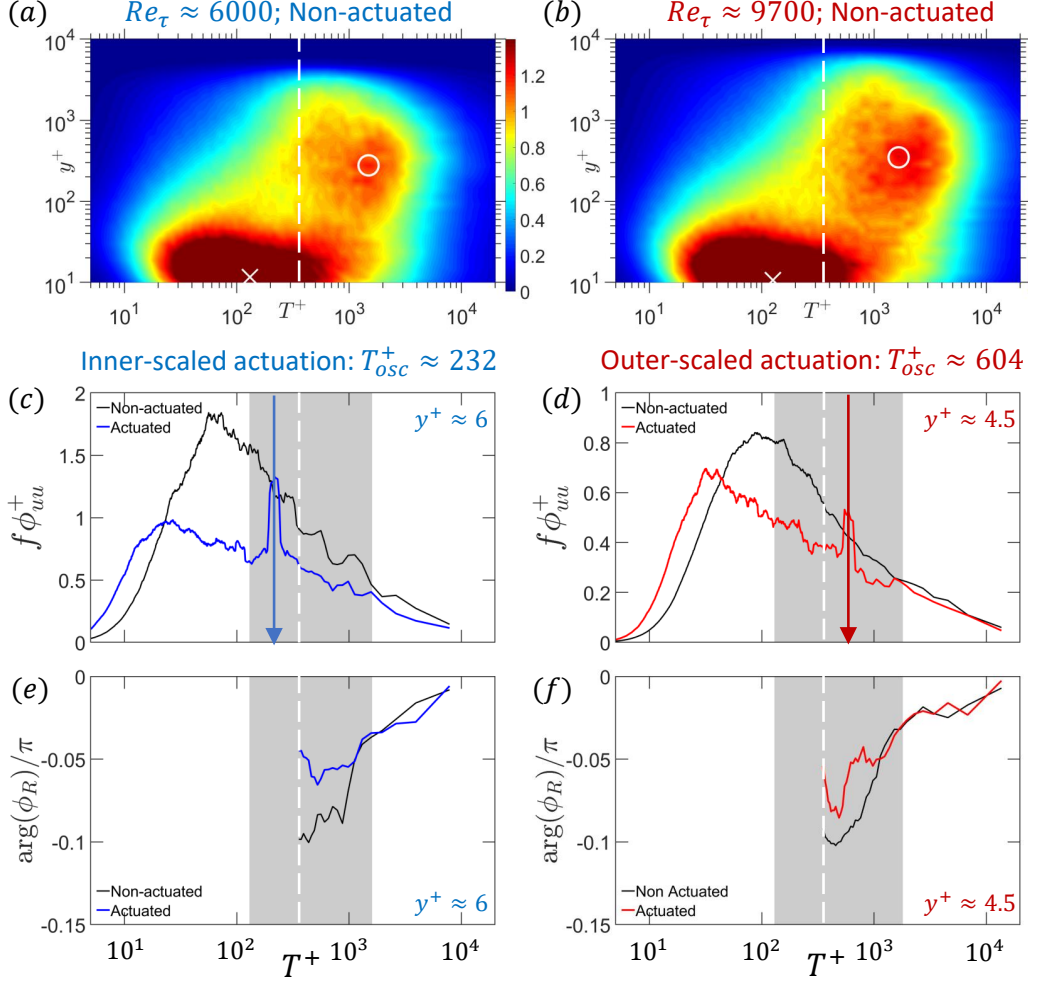


Figure 4: (a,b) Premultiplied  $u$ -spectrograms,  $f\phi_{uu}^+(y^+, T^+)$  for non-actuated (canonical) turbulent boundary layers acquired by Samie *et al.* (2018). (c,d) Premultiplied spectra of  $u$  ( $4.5 \leq y^+ \leq 6$ ) with and without wall-actuation for a specific (c) ISA and (d) OSA case. (e,f) Argument of the co-spectrum ( $\phi_R$ ) estimated for  $T^+ > 350$  for the same (e) ISA and (f) OSA case as in (c,d). Grey background represents the range of scales between the inner- (cross) and outer-peaks (circle) of the  $u$ -spectrograms in (a,b). The arrow in (c,d) indicates  $T_{osc}^+$ .

associated directly with the reduced mean phase difference between the triadically coupled scales (figure 2).

In addition, the maximum energy attenuation is always confined to the inner-scale region ( $T^+ \lesssim 350$ ) regardless of whether the spanwise oscillation targets the inner scales (figure 4c) or the outer scales (figure 4d). For example, for OSA, the spectra at  $T^+ \sim 100$  is attenuated by  $\sim 35\%$  on actuation, in contrast to  $\sim 10\text{--}15\%$  attenuation at  $T^+ \sim 600$ , which is closer to  $T_{osc}^+$ . These observations are consistent with the discussion based on figures 3(e,f), where for OSA the inner-scale contributions ( $u_i$ ) were found to be more severely attenuated than the outer-scale contributions. Hence, the manipulation of phase between the triadically coupled inner and outer scales (which enhances their coupling) appears to be the key to the success of the OSA

strategy, since it facilitates a substantial attenuation of the major drag contributing inner-scales despite the flow being actuated at the outer-scales (at much lower power).

While the increase in magnitude of the cross-talk term with DR in figure 3(d) supports the above arguments, it only gives an average estimate of the phase difference between all triadically coupled inner and outer scales. Following Jacobi & McKeon (2013, 2017), a more direct means to quantify the change in phase relationship on a per-scale basis is the argument (*arg*) of the co-spectrum,  $\phi_R$ , computed between the outer-scales ( $u_o$ ) and the outer-scale envelope of the inner-scales ( $\epsilon_o(u_i)$ ), where  $\phi_R = \langle \widetilde{u_o}(T^+) \epsilon_o(\widetilde{u_i}^*(T^+)) \rangle$ . The envelope is estimated via the Hilbert transform, with  $\phi_R$  physically interpretable only for  $T^+ > T_c^+$ , per definition. Here,  $\phi_R$  is essentially a spectral equivalent of the amplitude modulation coefficient,  $R(\Delta t) = \overline{u_o(t)\epsilon_o(u_i(t + \Delta t))} / \sqrt{\epsilon_o^2(u_i)} \sqrt{u_o^2}$ , which Mathis *et al.* (2011) used to quantify the non-linear coupling between the inner and outer-scales. Duvvuri & McKeon (2015) gave an exact relationship linking  $R$  and the cross-term as:  $R\left(\sqrt{\epsilon_o^2(u_i)} \sqrt{u_o^2}\right) = 2u_i^2 u_o$ , indicating that  $\text{arg}(\phi_R)$  would represent the scale-specific phase difference between the outer- and triadically coupled inner-scales.

Figures 4(e,f) respectively show the change in scale-specific phase estimated for the same ISA and OSA cases as in figures 4(c,d). Clearly, the actuation reduces the phase between  $u_o$  and  $\epsilon_o(u_i)$  for both OSA and ISA cases. This change in phase occurs nominally in the same scale-range as the attenuation of their corresponding premultiplied spectra ( $f\phi_{uu}^+$ ). The results from figures 2–4, therefore, are consistent in suggesting that increasing DR, for both ISA and OSA strategies, is facilitated by enhanced inter-scale coupling emerging through their reduced phase differences.

#### 4. Concluding remarks

We find that the turbulent drag reduction (DR) achieved by spanwise wall oscillations, which provokes a broadband attenuation of drag-producing turbulent scales, is facilitated by the enhanced coupling between the inner and outer scales. This inter-scale coupling emerges through the manipulation of the phase relationship between these scales, wherein the actuation forces the entire range of energy-containing scales, from the inner (viscous) to the outer (inertial) scales, to be more ‘in-phase’. This forcing occurs regardless of whether the flow is actuated at  $T_{osc}^+$  corresponding to the *inner-scaled actuation* (ISA) or the *outer-scaled actuation* (OSA) pathways; both lead to a moderate DR for a high  $Re_{\tau_o}$  flow. The criteria to optimize this control scheme, hence, narrows down to the power required to actuate the flow, which at any given Reynolds number is much lower in the case of OSA than ISA, making OSA the more energy-efficient pathway to high Reynolds number drag reduction (Marusic *et al.* 2021).

Furthermore, because the increase of near-wall  $\mathcal{S}_u$  with increasing  $Re_{\tau_o}$  is due solely to the  $3\overline{u_i^2 u_o}$  term (Mathis *et al.* 2011), the inner-outer coupling naturally increases with increasing  $Re_{\tau_o}$  for a canonical flow. Consequently, the drag reduction due to the OSA strategy is likely to be enhanced further at higher Reynolds numbers relevant to many applications, such as ships and aircraft.

## Acknowledgments

This research was funded through the Deep Science Fund of Intellectual Ventures and the Australian Research Council.

## Declaration of Interests

The authors report no conflict of interest.

## REFERENCES

AGOSTINI, L., TOUBER, E. & LESCHZINER, M. A. 2014 Spanwise oscillatory wall motion in channel flow: drag-reduction mechanisms inferred from DNS-predicted phase-wise property variations at  $Re_\tau = 1000$ . *J. Fluid Mech.* **743**, 606–635.

AKHAVAN, R., JUNG, W. & MANGIAVACCHI, N. 1993 Control of wall turbulence by high frequency spanwise oscillations. *AIAA paper* **93**, 3282.

CHANDRAN, D., ZAMPIRON, A., ROUHI, A., FU, M. K., WINE, D., HOLLOWAY, B., SMITS, A. J. & MARUSIC, I. 2022 Turbulent drag reduction by spanwise wall forcing. Part 2: High-Reynolds-number experiments. [arXiv:2211.03718](https://arxiv.org/abs/2211.03718) [physics.flu-dyn].

DECK, S., RENARD, N., LARAUFIE, R. & WEISS, P. 2014 Large-scale contribution to mean wall shear stress in high-Reynolds-number flat-plate boundary layers up to 13650. *J. Fluid Mech.* **743**, 202–248.

DUVVURI, S. & MCKEON, B. 2017 Phase relations in a forced turbulent boundary layer: implications for modelling of high Reynolds number wall turbulence. *Phil. Trans. R. Soc. A*: **375** (2089), 20160080.

DUVVURI, S. & MCKEON, B. J. 2015 Triadic scale interactions in a turbulent boundary layer. *J. Fluid Mech.* **767**, R4.

GATTI, D., STROH, A., FROHNAPFEL, B. & HASEGAWA, Y. 2018 Predicting turbulent spectra in drag-reduced flows. *Flow, Turbulence and Combustion* **100** (4), 1081–1099.

JACOBI, I. & MCKEON, B. J. 2013 Phase relationships between large and small scales in the turbulent boundary layer. *Exp. Fluids* **54** (3), 1–13.

JACOBI, I. & MCKEON, B. J. 2017 Phase-relationships between scales in the perturbed turbulent boundary layer. *J. Turbulence* **18** (12), 1120–1143.

MARUSIC, I. & OTHERS 2021 An energy-efficient pathway to turbulent drag reduction. *Nat. Commun.* **12** (1), 1–8.

MATHIS, R., MARUSIC, I., HUTCHINS, N. & SREENIVASAN, K. R. 2011 The relationship between the velocity skewness and the amplitude modulation of the small scale by the large scale in turbulent boundary layers. *Phys. Fluids* **23** (12), 121702.

QUADRID, M. & RICCO, P. 2011 The laminar generalized Stokes layer and turbulent drag reduction. *J. Fluid Mech.* **667**, 135–157.

QUADRID, M., RICCO, P. & VIOTTI, C. 2009 Streamwise-travelling waves of spanwise wall velocity for turbulent drag reduction. *Journal of Fluid Mechanics* **627**, 161–178.

RICCO, P., SKOTE, M. & LESCHZINER, M. A. 2021 A review of turbulent skin-friction drag reduction by near-wall transverse forcing. *Prog. Aero. Sci.* **123**, 100713.

SAMIE, M., MARUSIC, I., HUTCHINS, N., FU, M. K., FAN, Y., HULTMARK, M. & SMITS, A. J. 2018 Fully resolved measurements of turbulent boundary layer flows up to  $Re_\tau = 20\,000$ . *Journal of Fluid Mechanics* **851**, 391–415.